Deep Learning-Assisted Locating and Sizing of a Coating Delamination using Ultrasonic Guided Waves

Junzhen Wang[a], Maximilian Schmitz[b], Laurence J. Jacobs[b,c], Jianmin Qu[a*]

[a]Department of Mechanical Engineering, Stevens Institute of Technology, Hoboken, New Jersey 07030, USA

[b]School of Civil and Environmental Engineering, Georgia Institute of Technology, Atlanta, Georgia 30332, USA

[c]George W. Woodruff School of Mechanical Engineering, Georgia Institute of Technology, Atlanta, Georgia 30332, USA

ABSTRACT

This article proposes a deep learning-assisted nondestructive evaluation (NDE) technique for locating and sizing a coating delamination using ultrasonic guided waves. The proposed technique consists of sending a propagating guided wave into a coated plate with a transducer and measuring the corresponding time-domain signals by receivers at several locations at downstream distances from the source transducer. The received time-domain signals are then provided to a trained machine-learning (ML) algorithm, which subsequently outputs the location and size of any delamination flaws between the transducer and receivers. Numerical simulations show that the proposed NDE technique yields accurate results with high throughput, once the ML algorithm is well trained. Although training the ML algorithm is time-consuming, this training only needs to be done once for a given sample configuration. The results of this article demonstrate that the proposed technique has great potential for characterizing delamination flaws in practical NDE and structural health monitoring (SHM) applications.

Keywords: Guided wave; delamination; machine learning; deep learning; nondestructive evaluation; structural health monitoring

1. INTRODUCTION

Thin coatings are commonly used to improve the corrosion, oxidation, heat conduction, and wear performances of many mechanical and civil structure components [1, 2]. For example, due to their superior high-temperature strength, silicon carbide fiber-reinforced SiC ceramic

*jqu5@stevens.edu, Phone: +1 (201) 216-5263, Fax: +1 (201) 216-8909

composites have been reported as a potential cladding material in nuclear power systems [3]. In such applications, delamination of the coating layer may occur due to a variety of reasons, including poor adherence to the substrate and differential thermal expansion between the coating and the substrate [4]. This kind of hidden damage can significantly reduce the benefits of coating and endanger the overall structural reliability and durability. Therefore, it is important to develop nondestructive techniques to assess coating delamination flaws in safety-critical engineering applications.

Ultrasonic guided waves are a powerful tool for nondestructive evaluation (NDE) and structural health monitoring (SHM) of layered structures because of their ability to propagate over long distances [5-8]. Numerous guided-wave-based SHM techniques have been developed for delamination inspection in plate-like structures. The most prevalent approach involves Lamb waves in a pitch-catch configuration, which often utilizes a transmitter-receiver pair for wave generation and reception. When the incident waves interact with a delamination, reflection, mode conversion, and transmission can take place at the same time [9]. After passing the delaminated region, a considerable amount of energy of the incident waves would be trapped inside the delamination area [10]. Consequently, the location of a delamination can be determined by the variation in time-of-flight [11], and the delamination size can also be inferred by the wave amplitude drop [12-14]. With the advancement of non-contact ultrasonic sensors, the full-wavefield images acquired by a scanning laser Doppler vibrometer (SLDV) can image the delamination profile through the local wavenumber estimation [15]. Although many guided wave NDE and SHM techniques have been developed to characterize delamination flaws, the effective use of these techniques is highly dependent on the operator's experience, and deep multi-domain knowledge is indispensable to interpreting the guided wave features. To address the challenge of operator dependence, automatic delamination detection methods have attracted more attention to reduce the reliance on human expertise.

Recently, the development of data-driven methods such as machine learning (ML) and deep learning (DL) have provided a promising approach to solving the inverse problem. Machine learning allows for the effective mapping of input guided-wave features with damage types, localization, and severity [16]. For example, Sikdar and Pal used the bag of visual words (BOVW) for the classification of the structural healthy and disbond conditions [17]. Delamination in composite plates can be accurately localized by applying the support vector

machine (SVM) algorithm combined with a sparse sensor array [18]. As a specialized subfield of machine learning, deep learning enables learning hierarchical features from raw data based on neural networks with multiple layers. One of the significant advantages of deep learning is that the interference introduced by manual feature selection can be avoided. In particular, the convolutional neural network (CNN) has been used widely and successfully in automatic damage identification [19-22]. For example, low-frequency vibration responses were fed into a CNN classifier to distinguish the existence of delamination in smart composite laminates [23]. Guided wave pulse-echo and pitch-catch active sensing signals were employed to train both 1D and 2D CNNs for delamination detection and localization [24]. In addition, a sensor network was further designed to facilitate a plurality of wave interrogation paths, serving as the training data for crack diagnosis [25]. The guided wave delay-and-sum (DAS) images can also be trained with the proposed CNN architecture to predict the flaw locations and sizes [26].

Investigations using ultrasonic guided waves assisted by deep learning algorithms have been extensively performed to evaluate structural integrity. However, the training sources are still very limited in the open literature, including temporal signals [24, 25, 27], spectral distributions [18, 28, 29], time-frequency scalegrams [18, 29, 30], frequency-wavenumber information [31], DAS images [26], and full wavefield images [32].

This study advances the existing ML/DL methodologies by taking full advantage of time-space images to localize and size delamination in coated plates. The time-space diagram records wave-propagation patterns in a specific direction, endowed with guided wave dispersion characteristics [33] and attenuation behavior [34] for the intact case. Many distinctive wave damage interaction phenomena, e.g., mode conversion and wave reflection, can also be captured by the time-space representation [35]. Therefore, the time-space images contain wave signatures in both temporal and spatial domains, possessing tremendous potential for damage detection in NDE and SHM applications. This paper further explores its capability to predict the location and size of coating delamination with the combination of deep neural networks. This provides a feasible approach to solving the inverse problem of damage evaluation.

The paper is arranged as follows. Section 2 conducts finite element simulations for the forward computation of time-space images, with an emphasis on the advantages of utilizing deep neural networks to automatically evaluate delamination. In Section 3, a convolutional neural network is proposed, and the prediction results are presented. The out-of-range delamination is

further tested to showcase the effective prediction of delamination whose locations are not included in the training dataset. Section 4 concludes the paper with a summary and some observations.

2. Numerical Simulation for the Forward Problem

In this section, the forward problem of guided wave propagating through a coated plate is simulated by carrying out numerical computations using the finite element method. The numerical model is constructed to simulate guided wave generation, propagation, interaction with a delamination, and reception. Consequently, the time-space image can be obtained for each delamination condition.

2.1 Finite Element Modeling

We consider a double-layer plate consisting of a zirconium alloy substrate with a chromium coating. The corresponding material properties can be found in Table 1. The thickness of the substrate is modeled as 1 mm, and the coating thickness is one-fifth of that of the substrate (i.e., 0.2 mm). To select a guided wave mode for interrogation that is sensitive to delamination, a dispersion analysis is initially performed.

Table 1: Material properties for the coated plate [31].

Layer	Material	Young's modulus (GPa)	Poisson's ratio	Density (kg/m^3)
Coating	Chromium	279	0.21	7190
Substrate	Zircaloy-4	99.3	0.37	6560

Dispersion curves and mode shapes can be analytically computed by solving the characteristic equation for multi-layered plates [8, 36, 37]. Figure 1 shows the phase velocity dispersion curve as well as the displacement mode shapes of the two fundamental wave modes at 750 kHz. Since these modes are neither purely symmetric nor purely anti-symmetric [37], we name them the quasi-fundamental anti-symmetric (qA0) and the quasi-fundamental symmetric (qS0) based on their similarities with their counterparts in an isotropic plate. It is obvious that the qA0 mode has a comparatively larger out-of-plane displacement at the interface. Thus, it is plausible that the qA0 mode is more sensitive to delamination located at the interface. Another

benefit of choosing the qA0 mode for delamination inspection is that many receivers such as PZT transducers and SLDV are also most sensitive to out-of-plane displacements [38]. Therefore, the qA0 wave is selected here as the interrogation mode to interact with damage in the following finite element simulations.

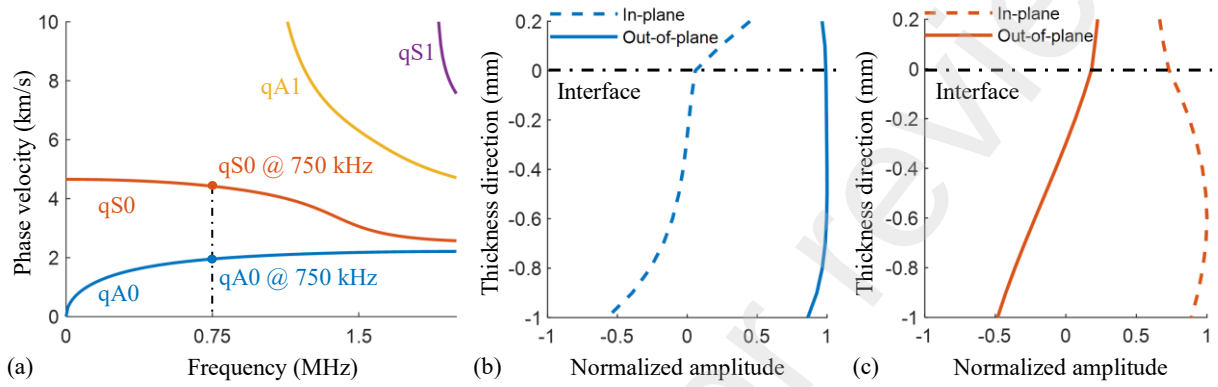

Figure 1: Guided wave-propagation features in the coated plate: (a) phase velocity dispersion curve; (b) displacement mode shape of mode qA0 at 750 kHz; (c) displacement mode shape of mode qS0 at 750 kHz.

The commercial finite element method (FEM) package ANSYS 19.0 was used to simulate the guided wave motion in the coated plate. Figure 2 shows the constructed 2D transient dynamic numerical model. The length of the coated plate was 410 mm. The excitation signal was a 5-count Hanning window modulated tone burst waveform centered at 750 kHz, scaled by the in-plane and out-of-plane displacement profiles of the qA0 mode at the same frequency. Distributed forces were simultaneously imposed on the nodes along the left boundary of the plate to generate the qA0 mode [39]. In this case, the time step Δt was calculated following the guideline [40]

$$\Delta t = \frac{1}{20 f} \tag{1}$$

where f is the frequency of interest. The quadrilateral element type PLANE182 was used to mesh the entire plate. The determination of element size l_e also followed the recommendation [40]

$$l_e = \frac{\lambda_{\min}}{20} \tag{2}$$

where $\lambda_{\min}$ is the wavelength of the qA0 mode at 750 kHz, which can be computed from the phase velocity dispersion curve. The corresponding mesh size was 0.1 mm in both in-plane and out-of-plane directions to warrant computational accuracy. A total of 1,000 sensing points were used on the top surface of the plate to receive the guided wave responses. The first sensing point was located at x = 150 mm, and each sensing point was spaced 0.2 mm apart, allowing for capturing a 200-mm wavefield propagation distance to create the time-space images. Non-reflective boundary (NRB) was implemented at the end of the plate [41]. The coverage of NRB was more than twice as long as the wavelength of the qA0 mode, which could guarantee the effective absorption of boundary reflections.

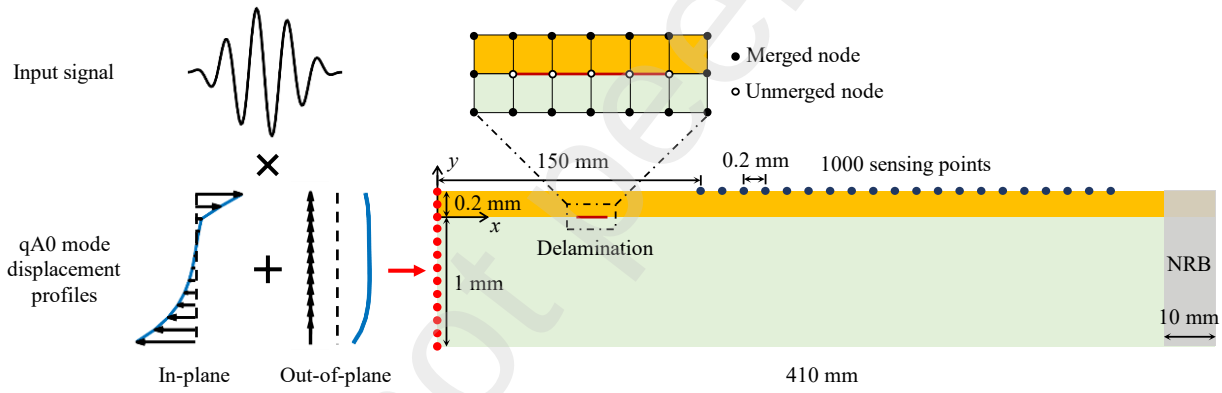

Figure 2: Finite element model for guided wave active sensing.

The callout in Figure 2 shows the region containing a delamination flaw. The nodes on each side of the interfacial flaw were unconnected, simulating the two free surfaces along the interface. Such modeling technique can be found in the open literature [24, 42].

2.2 Analysis of Simulation Results

To illustrate the influence on guided wave features induced by the existence of delamination, a pristine model was first simulated with the same actuation and sensing configuration. Figure 3 shows the temporal signal and time-space representation of the pristine case. The time domain signal of the out-of-plane displacement component was recorded at the node located at x = 150

mm. Two separate wave packages can be identified. They are the qS0 and qA0 modes, respectively. Their propagating trajectories were further captured by the time-space image. The reason why a low amplitude qS0 mode was excited is that the mode shape of the qA0 mode with the excitation bandwidth varies slightly with the frequency. Thus, the generation of the dominant qA0 mode and weak qS0 mode mimics the actual signals observed in practice. In addition, the time-space representation nicely depicted the guided wave dispersive characteristic based on the wave-package propagating patterns. In this case, it can be seen that the qS0 mode is more dispersive than the qA0 mode in terms of both phrase and group velocities.

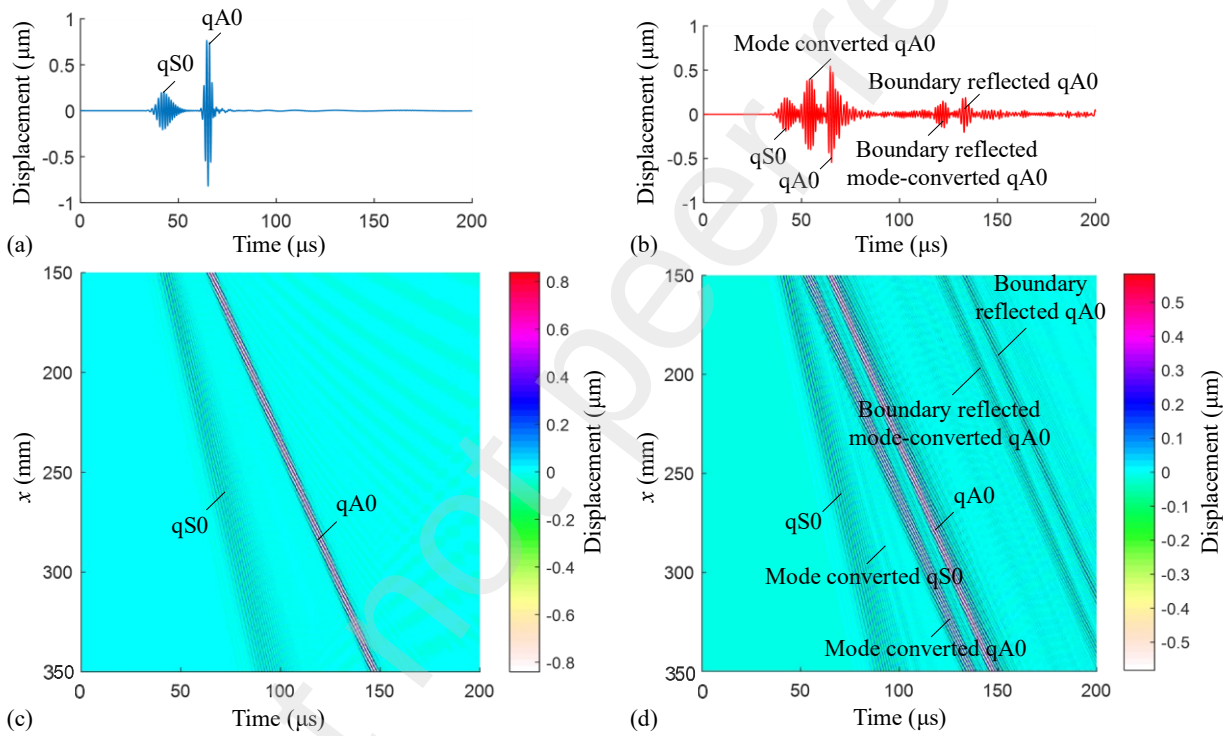

Figure 3:Simulation results of the pristine plate and the plate with a 2-mm long delamination located at x = 80 mm: (a) temporal signal of the pristine plate; (b) temporal signal of the damaged plate; (c) time-space image of the pristine plate; (d) time-space image of the damaged plate.

When the incident wave interacts with the delamination flaw, the scattered wave field becomes more complex. Figure 3 shows the time domain signal and time-space image of the coated plate with a 2-mm long delamination located at x = 80 mm (measured from the left tip of

the flaw). The amplitude of the main incident wave packages decreased significantly because the wave energy was trapped within the delaminated region. In addition, mode conversion also took place that generated an additional qA0 mode between the transmitted qS0 and qA0 modes. It should be noted that the weaker mode-converted qS0 mode can also be found immediately behind the transmitted qS0 mode in the time-space image. Therefore, in this case, the mode conversion phenomenon from the qS0 mode to the qA0 mode was more obvious than its counterpart. Furthermore, the mode-converted qA0 wave and the reflected qA0 mode from the delamination flaw experienced another reflection from the left boundary of the plate, respectively. All these wave components are contained in the temporal and spatial representations.

Before closing this section, it is worth noting the advantages of using guided wave time-space images assisted by neural networks for solving the inverse problem. The following three remarks can be made:

(1) The guided wave baseline (pristine sample) data are no longer required to determine the locations and sizes of any damage. That is to say, the proposed methodology is a baseline-free technique that evaluates the structural flaws without referring to the pristine condition.

(2) Many current NDE methods can only achieve quantitative evaluation by associating the damage characteristics with a predefined damage index. However, the technique proposed here enables direct measurement of precise localization and size of any coating delamination flaws.

(3) Unlike many existing approaches where care must be taken to generate desired wave modes to simplify the interpretation of the received signals, the technique proposed here utilizes the full wave fields with all existing components (e.g., mode-converted waves, reflected waves, and scattered waves).

3. Neural Network for Inverse Problem

In this section, the inverse problem is solved through a neural network regression algorithm. The processing of time-space images obtained from the forward computation is illustrated. Not only the in-range dataset but also out-of-range images are tested to evaluate the capability of the trained neural network.

3.1 Dataset Preparation

Neural networks are a subfield of machine learning, and they are at the heart of deep learning algorithms. Among the different algorithms, the convolutional neural network (CNN) stands out because of its extraordinary performance with images [21]. It processes the image by operating the convolution of the neighboring pixels. Throughout the layers of the CNN architecture, it can gradually recognize greater portions of the image and ultimately identify the intended object.

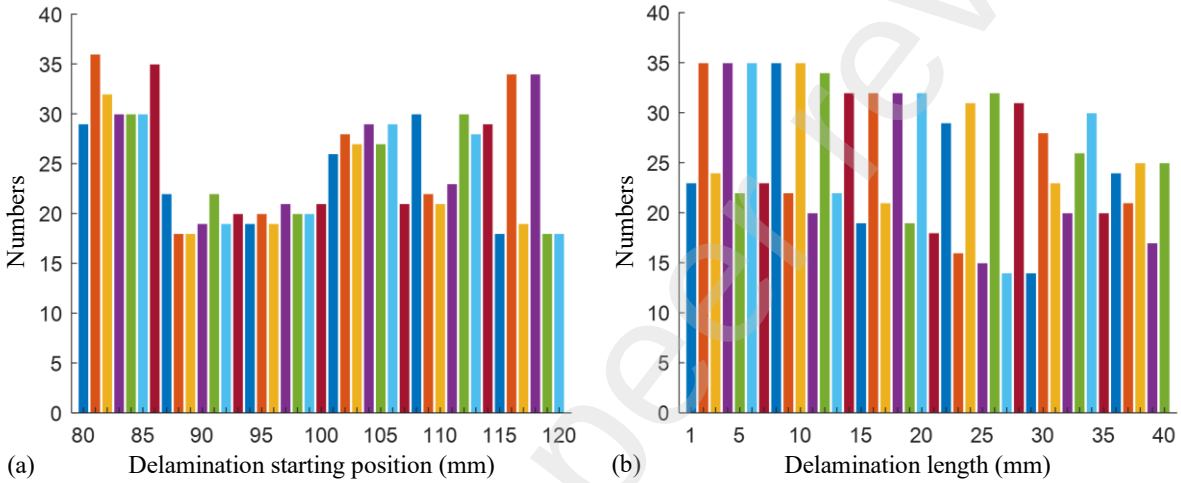

Figure 4: Dataset distribution in terms of delamination starting positions and lengths: (a) delamination starting positions; (b) delamination lengths.

To obtain the time-space images needed for training the CNN, a total of 1,250 FEM simulations were conducted with varying delamination sizes and locations, see Figure 4. The delamination positions started from 80 mm to 120 mm with an incremental interval of 1 mm. The number for each starting position was randomly distributed. The delamination lengths spanned from 1 mm to 40 mm with an increment of 1 mm. For each pair of delamination starting position and length, we can generate a time-space image. To test the robustness of the model, the simulation results of the cases where the delamination was partially underneath the sensing area were also included in the total dataset.

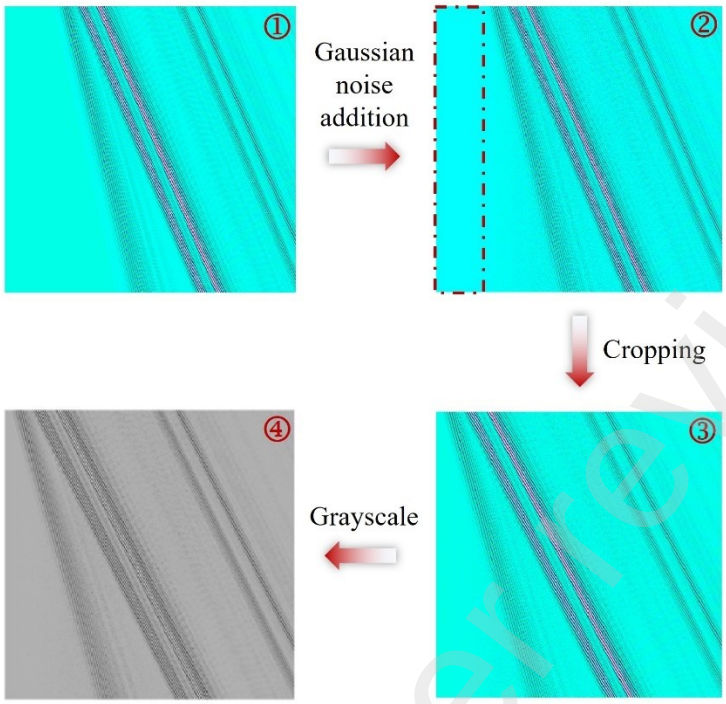

Figure 5: Process of dataset preparation.

To effectively handle the large amount of data generated by the FEM simulations, several data augmentation approaches were used in this study including image flipping, image rotation, image shifting, and the addition of Gaussian noise [30]. Specifically, 4-different levels of random Gaussian noise were added to the raw signals to account for uncertainty and noise in the experimental data, i.e., the signal-to-noise ratio (SNR) equal to 25 dB, 30 dB, 35 dB, and 40 dB. Consequently, the total number of datasets became 5,000. Figure 5 shows the 3 steps used to process the dataset. Since nothing is recorded by the receiver until the incident wave arrives, the corresponding area in the time-space image does not provide useful information for delamination identification. Therefore, the second step is to crop this part and retain meaningful guided wave patterns. Finally, the 3-channel color image is converted to a single-channel grayscale image. One advantage of using the one-channel intensity representation is that the neural network only needs to process a smaller amount of data, which can substantially reduce the computational time. The resolution of the final time-space image used was 252 × 252, enabling capturing even small changes in the image.

3.2 Neural Network Architecture and Training Details

The CNN architecture utilized in this study is shown in Figure 6. The input to the CNN is the 1-channel grayscale time-space image with 252 × 252 pixels. There are 6 convolutional layers in the network, all are followed by the ReLu [43] activation function and a batch normalization layer [44]. After each convolution layer, a max-pooling layer was added to the network. The 2 by 2 square kernels were employed to reduce the image pixels in half along both directions. After 6 rounds of convolution and pooling, the image size was reduced to 4 × 4, and the number of channels increased to 256. Subsequently, the extracted features were flattened and fed to a fully connected network with 1,024 neurons in the hidden layer. The regression output is the value of the delamination starting position or its length. It means that the location and size of the simulated delamination are independently characterized by the neural network. Detailed configuration of the proposed CNN architecture is shown in Table 2.

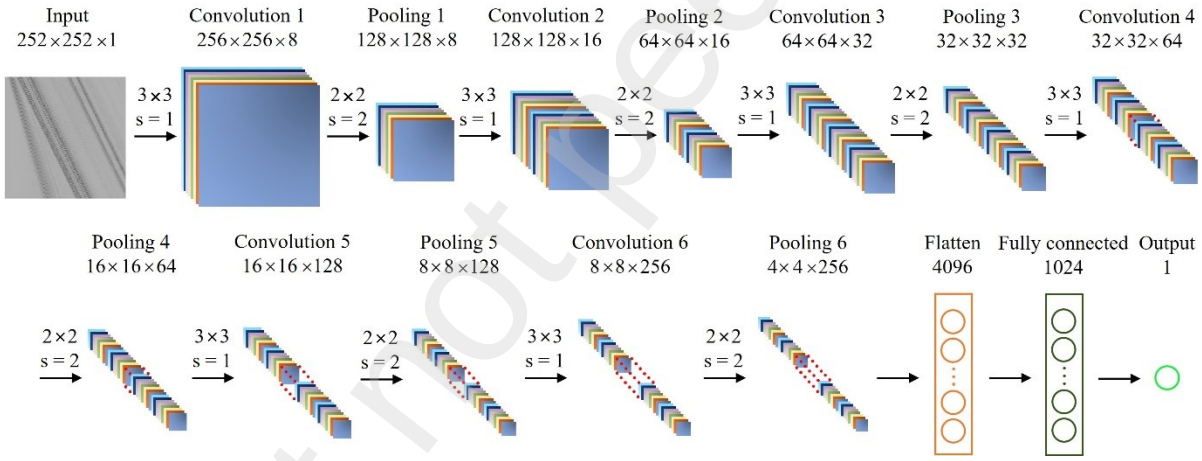

Figure 6: The proposed CNN architecture.

Table 2: The proposed neural network configuration.

Layer name	Layer description
Input	252 × 252 1-channel time-space image
Convolution 1, pooling 1	Convolution filter 3 × 3, strides 1, padding 3 Number of filters 8, ReLu, batch normalization Max pooling filter 2 × 2, strides 2

Convolution 2, pooling 2	Convolution filter 3 × 3, strides 1, padding 1 Number of filters 16, ReLu, batch normalization Max pooling filter 2 × 2, strides 2
Convolution 3, pooling 3	Convolution filter 3 × 3, strides 1, padding 1 Number of filters 32, ReLu, batch normalization Max pooling filter 2 × 2, strides 2
Convolution 4, pooling 4	Convolution filter 3 × 3, strides 1, padding 1 Number of filters 64, ReLu, batch normalization Max pooling filter 2 × 2, strides 2
Convolution 5, pooling 5	Convolution filter 3 × 3, strides 1, padding 1 Number of filters 128, ReLu, batch normalization Max pooling filter 2 × 2, strides 2
Convolution 6, pooling 6	Convolution filter 3 × 3, strides 1, padding 1 Number of filters 256, ReLu, batch normalization Max pooling filter 2 × 2, strides 2
Fully connected	Input 4096, output 1024 Input 1024, output 1

The processed datasets were randomly shuffled and assigned to the training sets and the evaluation sets. In this study, 85% of the data were used for training, 10% for validation, and 5% for testing. The training was performed in MATLAB with tuned hyperparameters presented in Table 3. The Adam optimizer was utilized for fast calculation, and the regression model was trained for up to 100 epochs. The initial learning rate was set as 2×10^{-5}, and when it came to the 50^{th} epoch, the learning rate was multiplied by the drop factor. This type of piecewise learning rate schedule can yield a fast convergence in the beginning and ensure a high validation accuracy in the final stage [45]. The classic mean squared error (MSE) loss L_{MSE} was used to quantify the difference between the target and predicted output value, which is defined as [30]

$$L_{MSE} = \frac{1}{N}\sum_{n=1}^{N}\left(y_n - \hat{y}_n\right)^2 \tag{3}$$

where N stands for the batch size; y_n represents the simulated delamination parameter; $\hat{y}_n$ is the

predicted value. In this study, the batch size was tuned and eventually determined as 64.

Table 3: Hyperparameters of the training process.

Hyperparameters	Optimizer	Epoch	Initial learning rate	Learning rate schedule	Learning rate drop factor	Learning rate drop period	Loss function
Value	Adam	100	2×10^{-5}	Piecewise	0.1	50	MSE

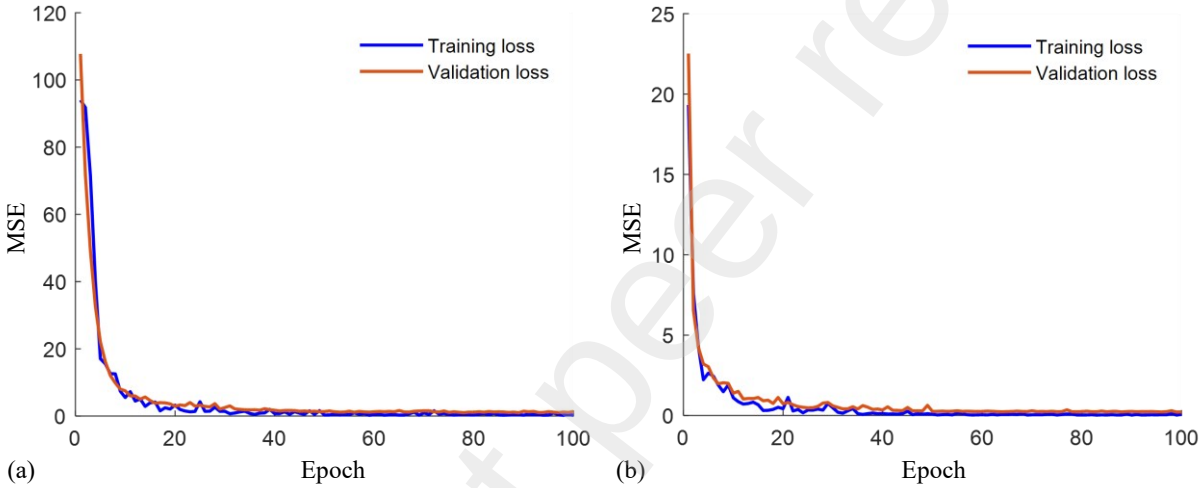

Figure 7: Training performances: (a) delamination localization; (2) delamination sizing.

Figure 7 shows the training and validation losses for delamination localization and sizing, respectively. The curves for each delamination inspection look quite similar to each other. They experienced a rapid decrease within the beginning several epochs, and then slowly declined reaching a relatively small value. This demonstrates that no overfitting phenomenon happens in each independent training process.

3.3 Delamination Prediction Results

To evaluate the prediction accuracy, mean absolute percentage error (MAPE) denoted by L_{MAPE} was used, which takes the form of [24]

$$L_{MAPE} = \frac{1}{N}\sum_{n=1}^{N}\frac{y_n - \hat{y}_n}{y_n}. \quad (4)$$

It is seen that Eq. (4) calculates the comparative deviation between the simulated and predicted damage parameters. Table 4 displays the MAPE of our prediction on the test dataset compared with another deep-learning model trained by temporal signals and time-frequency diagrams reported in [24]. Our proposed technique rendered much smaller errors for both delamination localization and sizing, respectively. This improvement is attributed to the spatial information of the wave motion.

Table 4: Comparison of deep learning methods using guided waves for delamination localization and sizing.

MAPE	Delamination location	Delamination length
Ours	1.00%	4.24%
Rautela and Gopalakrishnan [24]	8.50%	11.3%

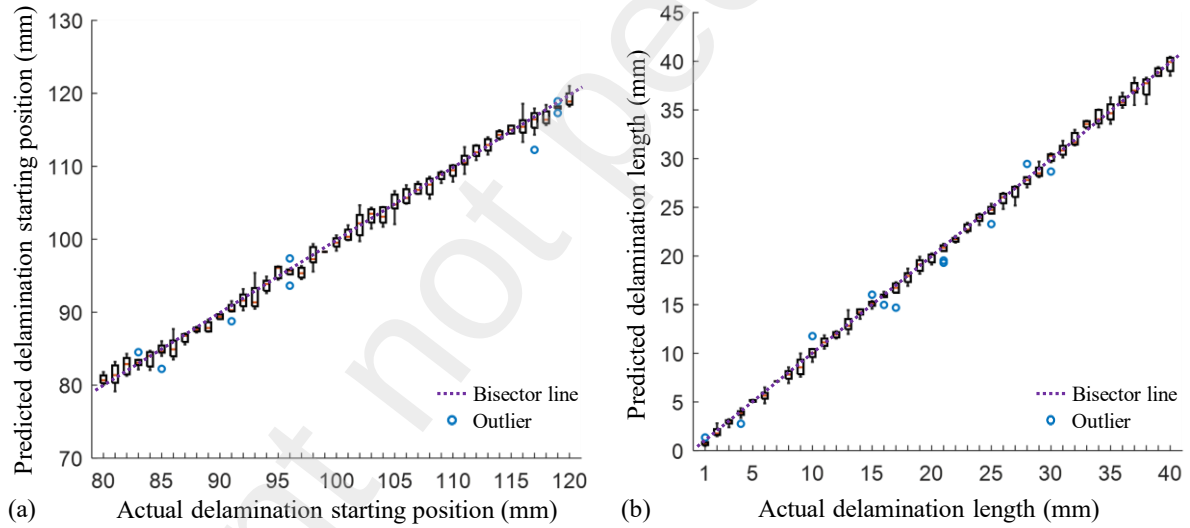

Figure 8: Prediction Results: (a) delamination localization; (b) delamination sizing.

Some detailed regression results are illustrated in Figure 8. Predicted delamination location and lengths are plotted using boxplots. It is seen that almost all the predicted values were on or very near the bisector line, with only a very few outliers (denoted by blue circles). These results demonstrate that the developed neural network is able to accurately predict the damage location and size.

3.4 Prediction of an Out-of-range Delamination

The CNN algorithm developed above was trained with datasets that contain a range of delamination locations and sizes. To test its robustness, consider if the CNN algorithm so trained is capable of predicting out-of-range damages (e.g., damage conditions outside of the range of the training data). To this end, we extended the existing time-space images by conducting the FEM simulations for the damaged model with out-of-range starting locations. For simplicity, we maintained the delamination lengths in the range between 1 mm and 40 mm, and the excitation and sensing system was also kept the same. Specifically, two sets of starting positions were simulated. They range from 75 mm to 79 mm and from 121 mm to 125 mm. The corresponding delamination lengths were randomly distributed in the original region.

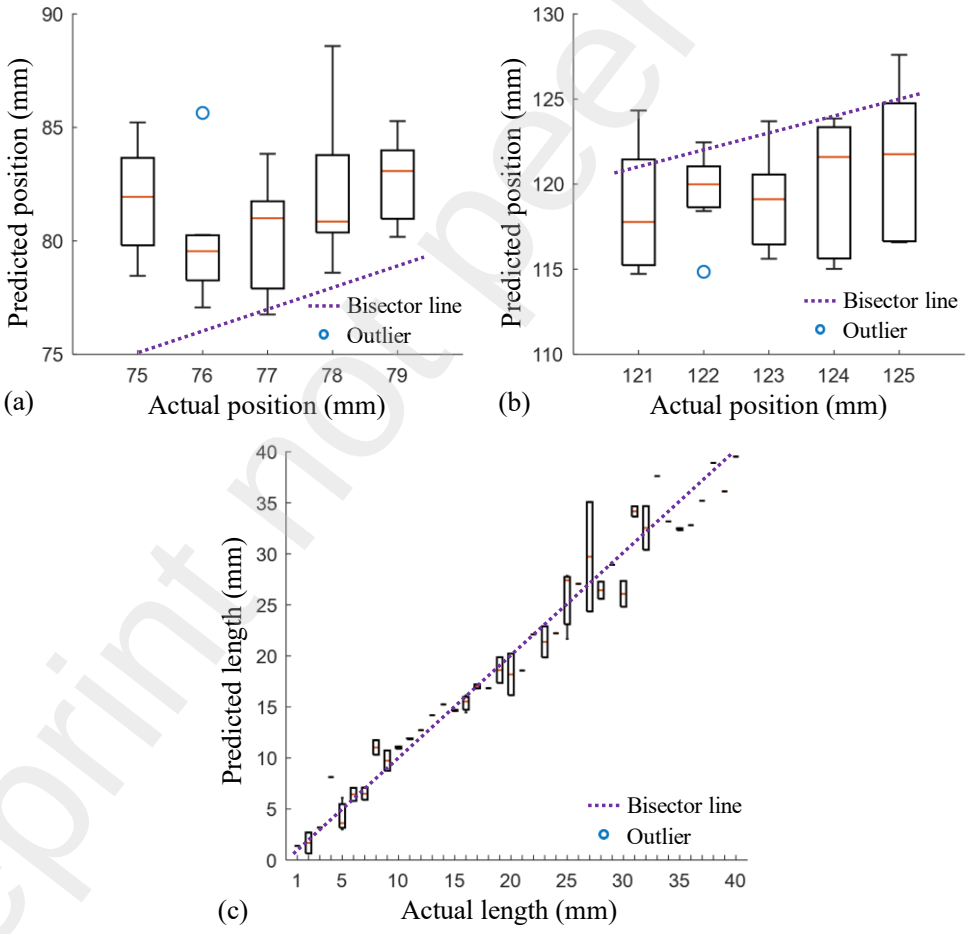

Figure 9: Prediction results of the extended test data: (a) delamination localization with their starting positions from 75 mm to 79 mm; (b) delamination localization with their starting positions from 121 mm to 125 mm; (c) delamination sizing.

Figure 9 shows the predicted results of the extended test data. Figure 9(a) and (b) show the regression for each set of delamination starting positions, respectively. Although most of the boxes shifted above or below the bisector line, the actual delamination positions can be approximately predicted. This demonstrates that the trained CNN developed here is capable of predicting out-of-range delamination locations with reasonable accuracy. We believe that such robustness is due to the fact that the time-space image can be reconstructed via sliding along the time axis for the cases of out-of-range delamination. Consequently, the trained CNN enables providing an effective tool to predict delamination flaws.

The predicted delamination lengths are shown in Figure 9(c). It is seen that most of the predictions are found across the bisector line, indicating that the size of delamination whose positions were outside the training data can be accurately predicted. In other words, the proposed method has the capability of predicting out-of-range delaminations.

We note that another aspect of the model's robustness is the ability to predict out-of-range delamination size. Unfortunately, the time-space images in this case exhibit quite different pixel distributions and the current CNN model is unable to predict the delamination length.

4. Summary and Conclusions

In this paper, we propose a novel NDE technique assisted by a deep learning algorithm based on a CNN architecture for automatic assessment of delamination locations and sizes in a double-layer plate. A key enabling element of this proposed technique is the development of a trained deep-learning CNN algorithm.

The development and training of the proposed CNN algorithm consists of several steps. First, we conducted numerical calculations using the FEM simulations to solve the forward problem, i.e., obtaining the interactions between guided waves and delamination flaws. The complex wave field induced by the delamination flaw was recorded by an array of receivers. The recorded signals were then processed to yield two-dimensional time-space images.

Next, these time-space images for varying delamination conditions were used to train the developed CNN. Once trained, the CNN can be used as a tool to predict the delamination location and size.

Finally, a large number of test datasets were used as input to the train CNN. The predicted delamination locations and sizes were then compared with the actual delamination locations and

sizes. The results show that our trained CNN achieved much more accurate predictions than many existing tools. Such improvement can be attributed to the high fidelity of the time-space images used in training and testing the CNN.

Further, to test the robustness of the trained CNN algorithm, we extended the test data by considering out-of-range delamination. The trained network is still able to precisely predict the lengths of delamination whose locations were outside the training dataset, and their locations can be approximately determined. These further demonstrated that the proposed technique and the trained CNN are robust and can be used to predict out-of-range delamination flaws.

ACKNOWLEDGEMENTS

This research was supported in part by the US Department of Energy through its Nuclear Energy University Programs, DE-NE0008943.

REFERENCES

[1] J.P. Chu, J.S.C. Jang, J.C. Huang, H.S. Chou, Y. Yang, J.C. Ye, Y.C. Wang, J.W. Lee, F.X. Liu, P.K. Liaw, Y.C. Chen, C.M. Lee, C.L. Li, C. Rullyani, Thin film metallic glasses: Unique properties and potential applications, Thin Solid Films, 520 (2012) 5097-5122.

[2] T. Qureshi, G. Wang, S. Mukherjee, M. Akibul Islam, T. Filleter, C.V. Singh, D.K. Panesar, Graphene-based anti-corrosive coating on steel for reinforced concrete infrastructure applications: Challenges and potential, Construction and Building Materials, 351 (2022) 128947.

[3] S.J. Zinkle, K.A. Terrani, J.C. Gehin, L.J. Ott, L.L. Snead, Accident tolerant fuels for LWRs: A perspective, Journal of Nuclear Materials, 448 (2014) 374-379.

[4] A.G. Evans, J.W. Hutchinson, The mechanics of coating delamination in thermal gradients, Surface and Coatings Technology, 201 (2007) 7905-7916.

[5] Z. Su, L. Ye, Y. Lu, Guided Lamb waves for identification of damage in composite structures: A review, Journal of Sound and Vibration, 295 (2006) 753-780.

[6] M. Mitra, S. Gopalakrishnan, Guided wave based structural health monitoring: A review, Smart Materials and Structures, 25 (2016) 053001.

[7] A. De Luca, D. Perfetto, A. De Fenza, G. Petrone, F. Caputo, Guided wave SHM system for damage detection in complex composite structure, Theoretical and Applied Fracture Mechanics, 105 (2020) 102408.

[8] J. Wang, J. Qu, Guided wave propagation in a double-layer plate with a nonlinear spring-interface, Ultrasonics, 137 (2024) 107189.

[9] C. Schaal, A. Mal, Core-skin disbond detection in a composite sandwich panel using guided ultrasonic waves, Journal of Nondestructive Evaluation, Diagnostics and Prognostics of

Engineering Systems, 1 (2018) 011006.
[10] H. Sohn, D. Dutta, J.Y. Yang, M. DeSimio, S. Olson, E. Swenson, Automated detection of delamination and disbond from wavefield images obtained using a scanning laser vibrometer, Smart Materials and Structures, 20 (2011) 045017.
[11] M. Liu, S. Chen, Z.Z. Wong, K. Yao, F. Cui, In situ disbond detection in adhesive bonded multi-layer metallic joint using time-of-flight variation of guided wave, Ultrasonics, 102 (2020) 106062.
[12] F. Lanza di Scalea, P. Rizzo, A. Marzani, Propagation of ultrasonic guided waves in lap-shear adhesive joints: case of incident a0 Lamb wave, The Journal of the Acoustical Society of America, 115 (2004) 146-156.
[13] K. Wang, M. Liu, W. Cao, W. Yang, Z. Su, F. Cui, Detection and sizing of disbond in multilayer bonded structure using modally selective guided wave, Structural Health Monitoring, 20 (2019) 904-916.
[14] H. Mei, M.F. Haider, R. James, V. Giurgiutiu, Pure S0 and SH0 detections of various damage types in aerospace composites, Composites Part B: Engineering, 189 (2020) 107906.
[15] J. Spytek, L. Ambrozinski, L. Pieczonka, Evaluation of disbonds in adhesively bonded multilayer plates through local wavenumber estimation, Journal of Sound and Vibration, 520 (2022) 116624.
[16] Z. Yang, H. Yang, T. Tian, D. Deng, M. Hu, J. Ma, D. Gao, J. Zhang, S. Ma, L. Yang, H. Xu, Z. Wu, A review on guided-ultrasonic-wave-based structural health monitoring: From fundamental theory to machine learning techniques, Ultrasonics, 133 (2023) 107014.
[17] S. Sikdar, J. Pal, Bag of visual words based machine learning framework for disbond characterisation in composite sandwich structures using guided waves, Smart Materials and Structures, 30 (2021) 075016.
[18] L. Tang, Y. Li, Q. Bao, W. Hu, Q. Wang, Z. Su, D. Yue, Quantitative identification of damage in composite structures using sparse sensor arrays and multi-domain-feature fusion of guided waves, Measurement, 208 (2023) 112482.
[19] A.K.u. Malikov, Y. Cho, Y.H. Kim, J. Kim, J. Park, J.-H. Yi, Ultrasonic assessment of thickness and bonding quality of coating layer based on short-time Fourier transform and convolutional neural networks, Coatings, 11 (2021) 909.
[20] H. Sun, L. Peng, S. Wang, S. Huang, K. Qu, Development of frequency-mixed point-focusing shear horizontal guided-wave EMAT for defect inspection using deep neural network, IEEE Transactions on Instrumentation and Measurement, 70 (2021) 1-14.
[21] S. Cantero-Chinchilla, P.D. Wilcox, A.J. Croxford, Deep learning in automated ultrasonic NDE – Developments, axioms and opportunities, NDT & E International, 131 (2022) 102703.
[22] J. Rao, F. Yang, H. Mo, S. Kollmannsberger, E. Rank, Quantitative reconstruction of defects in multi-layered bonded composites using fully convolutional network-based ultrasonic inversion, Journal of Sound and Vibration, 542 (2023) 117418.
[23] A. Khan, D.-K. Ko, S.C. Lim, H.S. Kim, Structural vibration-based classification and

prediction of delamination in smart composite laminates using deep learning neural network, Composites Part B: Engineering, 161 (2019) 586-594.
[24] M. Rautela, S. Gopalakrishnan, Ultrasonic guided wave based structural damage detection and localization using model assisted convolutional and recurrent neural networks, Expert Systems with Applications, 167 (2021) 114189.
[25] L. Lomazzi, M. Giglio, F. Cadini, Towards a deep learning-based unified approach for structural damage detection, localisation and quantification, Engineering Applications of Artificial Intelligence, 121 (2023) 106003.
[26] R. Miorelli, C. Fisher, A. Kulakovskyi, B. Chapuis, O. Mesnil, O. D'Almeida, Defect sizing in guided wave imaging structural health monitoring using convolutional neural networks, NDT & E International, 122 (2021) 102480.
[27] Q. Yuan, Y. Wang, Z. Su, T. Zhang, Quantitative damage evaluation of curved plates based on phased array guided wave and deep learning algorithm, Ultrasonics, 137 (2024) 107176.
[28] S. Kumar, M.R. Sunny, A novel nonlinear Lamb wave based approach for detection of multiple disbonds in adhesive joints, International Journal of Adhesion and Adhesives, 107 (2021) 102842.
[29] F. Gao, J. Hua, Damage characterization using CNN and SAE of broadband Lamb waves, Ultrasonics, 119 (2022) 106592.
[30] B. Feng, S. Cheng, K. Deng, Y. Kang, Localization of low-velocity impact in CFRP plate using time–frequency features of guided wave and convolutional neural network, Wave Motion, 119 (2023) 103127.
[31] M. Schmitz, J.-Y. Kim, L.J. Jacobs, Machine and deep learning for coating thickness prediction using Lamb waves, Wave Motion, 120 (2023) 103137.
[32] A.A. Ijjeh, S. Ullah, P. Kudela, Full wavefield processing by using FCN for delamination detection, Mechanical Systems and Signal Processing, 153 (2021) 107537.
[33] P. Wilcox, M. Lowe, P. Cawley, The effect of dispersion on long-range inspection using ultrasonic guided waves, NDT & E International, 34 (2001) 1-9.
[34] L. Yu, Z. Tian, Case study of guided wave propagation in a one-side water-immersed steel plate, Case Studies in Nondestructive Testing and Evaluation, 3 (2015) 1-8.
[35] C. Zhang, Z. Zhang, H. Ji, J. Qiu, C. Tao, Mode conversion behavior of guided wave in glass fiber reinforced polymer with fatigue damage accumulation, Composites Science and Technology, 192 (2020) 108073.
[36] A.M.A. Huber, M.G.R. Sause, Classification of solutions for guided waves in anisotropic composites with large numbers of layers, The Journal of the Acoustical Society of America, 144 (2018) 3236.
[37] E. Pan, J. Rogers, S.K. Datta, A.H. Shah, Mode selection of guided waves for ultrasonic inspection of gas pipelines with thick coating, Mechanics of Materials, 31 (1999) 165-174.
[38] C.T. Ng, M. Veidt, Scattering of the fundamental anti-symmetric Lamb wave at delaminations in composite laminates, The Journal of the Acoustical Society of America, 129 (2011) 1288-1296.

[39] X. Cao, L. Zeng, J. Lin, J. Hua, A correlation-based approach to corrosion detection with Lamb wave mode cutoff, Journal of Nondestructive Evaluation, 38 (2019) 87.
[40] F. Moser, L.J. Jacobs, J. Qu, Modeling elastic wave propagation in waveguides with the finite element method, NDT & E International, 32 (1999) 225-234.
[41] J. Wang, Y. Shen, D. Rao, W. Xu, Physical-virtual time reversing of nonlinear Lamb waves for fatigue crack detection and quantification, Mechanical Systems and Signal Processing, 160 (2021) 107921.
[42] O.K. Ihesiulor, K. Shankar, Z. Zhang, T. Ray, Validation of algorithms for delamination detection in composite structures using experimental data, Journal of Composite Materials, 48 (2013) 969-983.
[43] V. Nair, G.E. Hinton, Rectified linear units improve restricted boltzmann machines, in: Proceedings of the 27th international conference on machine learning (ICML-10), 2010, pp. 807-814.
[44] S. Ioffe, C. Szegedy, Batch normalization: Accelerating deep network training by reducing internal covariate shift, in: International conference on machine learning, pmlr, 2015, pp. 448-456.
[45] W. Li, L. Zhang, C. Wu, Z. Cui, C. Niu, A new lightweight deep neural network for surface scratch detection, The International Journal of Advanced Manufacturing Technology, 123 (2022) 1999-2015.